-RESEARCH PAPER-

International Journal of Mining and Geo-Engineering

IJMGE

IJMGE 57-3 (2023) 267-274

DOI: 10.22059/IJMGE.2023.353516.595018

Edge detection of geological structures based on a logistic function: a case study for gravity data of Western Carpathians

Ahmad Alvandi [a, *], Hazel Deniz Toktay [b], Vahid E. Ardestani [a]

[a] *Institute of Geophysics, University of Tehran, Tehran, Iran.*

[b] *Department of Geophysical Engineering, Istanbul University - Cerrahpasa, Istanbul, Turkey.*

Article History:

Received: 06 January 2023.

Revised: 25 March 2023.

Accepted: 07 May 2023.

ABSTRACT

Magnetic and gravity anomalies have spatially overlapping fingerprints from many buried sources that differ in shape, depth, density contrast, magnetization intensity, and direction. Geophysicists have developed a suite of image enhancement filter algorithms that accurately represent the geometry and detail of subsurface features. Edge enhancement filters are high-pass filters that emphasize potential field anomalies, horizontal lateral edges, and the horizontal location of buried sources, i.e., specific combinations of directional derivatives of gravity and magnetic fields. Lateral edge enhancement filters (e.g., THG, AS, TA, TM, LTHG, IL, and ILTHG) were investigated using Gaussian noise on synthetic magnetic and gravity field data. The results show that LTHG and IL perform better than the other procedures. The ILTHG filter defined with the logistic function does not have the required accuracy and capability to determine the lateral boundaries. In addition, the filters were examined using real gravity field data from the Western Carpathians area in Slovakia. The primary and secondary faults in the western and southern Tribeč Mountains and the secondary faults and geological formations in the Pohronský Inovec Mountains are recognizable in the LTHG and IL images. The results of the LTHG and IL maps will allow us to improve the qualitative interpretation of gravity anomalies in studying the structural and tectonic geology of the Slovak Tribeč and Pohronský Inovec Mountains.

Keywords: *Edge enhancement filter, Gravity data, Logistic function, Slovakia territory.*

1. Introduction

The methods of potential field measurement (gravity and magnetic) are the oldest methods used for determining the nature, and the structure of the earth. Despite the advancement of complementary survey methods, some of which have improved the quality of the subsurface, gravity and magnetic field methods continue to play an essential and often crucial role in exploring hydrocarbons and minerals, and also in the study of geological and such structures [1]. In recent decades, various techniques have been developed for processing and analyzing potential field data to obtain better results and higher resolution [2]. Image enhancement filtering techniques are used to aid in interpreting gravity and magnetic anomalies [2, 3]. These techniques are typically used to estimate the lateral edges of gravity and magnetic field data. Most procedures rely on the maximum or minimum amount of directional derivatives or a combined form of them (e.g., total horizontal gradient, tilt derivative, theta map, the logistic function of total horizontal gradient, improved logistic function, and improved total horizontal derivative logistic function).

Further development of these filters to detect the effects of deeper sources or lower amplitude causative subsurface structures in addition to shallower sources or larger amplitude anomalies has resulted in more effective filters [4]. Therefore, a more accurate and complete interpretation can be provided with these filters. Also, these filters can be used in inverse modeling as additional and precise information when producing geologic models. The following (Methodology) represents edge detection algorithms and their mathematical equations.

2. Methodology

The total horizontal gradient (THG) filter proposed by Cordell and Grouch (1985), which uses the directional field derivatives, is the most commonly used filter. The THG approach can be calculated as follows:

$$THG = \sqrt{\left(\frac{\partial P}{\partial x}\right)^2 + \left(\frac{\partial P}{\partial y}\right)^2} \quad (1)$$

where P is the amount of the gridded gravity or magnetic anomaly reduced to the pole, $\frac{\partial P}{\partial x}$ and $\frac{\partial P}{\partial y}$ are the horizontal derivatives in the X and Y directions, respectively. The maximum value of THG can play a cruciaql role in indicating the edges of the buried source.

In the work conducted by Nabighian (1984), an extension of the two-dimensional analytic signal to a three-dimensional context was undertaken. This extension revealed that the Hilbert transform of gravity or magnetic field not only adheres to but also fulfills the Cauchy-Riemann equations [5]. The formulation introduced by Roest et al. (1992) encompassed an extension of the previously calculated analytic signal in a horizontal plane to a three-dimensional domain. This extension elucidated that the three-dimensional analytic signal can be expressed as follows:

$$AS = \sqrt{\left(\frac{\partial P}{\partial x}\right)^2 + \left(\frac{\partial P}{\partial y}\right)^2 + \left(\frac{\partial P}{\partial z}\right)^2} \quad (2)$$

In equation (2), $\frac{\partial P}{\partial z}$ represensts the vertical gradient of the gravity anomaly or reduced to the pole magnetic anomaly. One major reason

* Corresponding author. *E-mail address:* aalvandi@ut.ac.ir (A. Alvandi).

for using the AS approach in potential field data interpretation is its ability to disregard the direction of source magnetization. This method also lets us identify the edges of buried sources based on the highest amplitude of the analytical signal, making it quite valuable in potential field data analysis. [6]. Certainly, this scenario does not hold for three-dimensional sources. [7]. The highest value within the analytic domain does not precisely correspond to the source location, leading to inaccuracies in determining the source's horizontal boundaries [8, 9]. Both the analytical signal and total horizontal gradient methods prove inadequate in delineating the edges of deep and embedded structures [4]. To address these limitations, the introduction of local phase filters came into play.

Miller and Singh (1994) introduced the tilt angle or derivative technique to enhance edges' delineation in deeply and shallowly buried structures [10–11]. Subsequent research, conducted by others such as Salem et al. (2007, 2008) and Fairhead et al. (2008), has extended this filter to conduct a more reliable one. This approach has garnered significant attention owing to its fundamental and pragmatic simplicity [11]. The local phase or tilt angle, sometimes referred to as the tilt derivative [1, 11], is defined as follows:

$$TA=\tan^{-1}\left[\frac{\frac{\partial P}{\partial z}}{\sqrt{\left(\frac{\partial P}{\partial x}\right)^2+\left(\frac{\partial P}{\partial y}\right)^2}}\right] \quad (3)$$

The interpretability of the tilt angle (TA) surpasses that of the AS and THG maps. Nevertheless, it is important to acknowledge that this filter also exhibits relative limitations in accurately defining the boundaries of deeply situated and embedded causative subsurface structures [5]. The TA possesses the advantage of being independent of vertical and horizontal derivatives of the potential field, thus rendering it less susceptible to noise in comparison to alternative algorithms [1]. TA values consistently span the range of -90° to +90°. Positive TA values are prominent over a causative source, transitioning through 0° around or in proximity to the horizontal border of a concealed source, and displaying negativity beyond the extent of the causative source region [10, 11].

Another edge enhancement filter is the theta angle or theta map (Wijns et al., 2005). It applies the analytic signal to normalize the THG. The TM gives good results, but the detected edges tend to be scattered [12]. The theta angle procedure is defined as [16]:

$$TM=\cos^{-1}\frac{\sqrt{\left(\frac{\partial P}{\partial x}\right)^2+\left(\frac{\partial P}{\partial y}\right)^2}}{|AS|} \quad (4)$$

In recent years, starting from 2019, there have been advancements in edge-detection filters using a mathematical concept called the logistic or sigmoid function. These filters stand out because they can identify the boundaries of both shallow and deep structures at a higher level of detail at the same time. They achieve this by finding a balance between the boundaries of these different layers using variations of the logistic function applied to the total horizontal gradient. This helps geologists distinguish geological features more accurately [13, 14, and 15]. The logistic function is similar to the arctangent function and plays a key role in creating these filters. In this study, researchers explored three different filters based on the logistic function. Pham et al. (2019) used one of these filters, called the logistic function of the total horizontal gradient (LTHG), to pinpoint the edges of gravity and magnetic anomalies. Here's how LTHG is defined [13]:

$$LTHG=\left[1+\exp\left(-\frac{\frac{\partial THG}{\partial Z}}{\sqrt{\left(\frac{\partial THG}{\partial x}\right)^2+\left(\frac{\partial THG}{\partial y}\right)^2}}\right)\right]^{-\propto} \quad (5)$$

In equation 5, the alpha value (∝) is the positive constant, ranging from 2-10 [20]. This filter was first applied by Pham et al. (2019) in order to conduct the edge detection techniques on potential field data. The method provides maximum amplitudes over the causative sources. The filter is also able to balance the visible edges showing large and small amplitudes [2, 4, 13].

To enhance the resolution of LTHG maps, the improved logistic filter (IL) was introduced. The key advantage of the IL algorithm lies in its ability to generate high-resolution and distinct images without generating false edges in the resulting visuals [2, 14]. The definition of IL is outlined as follows [14]:

$$IL=\frac{1}{1+\exp\left[-\alpha\left(\left(\frac{\frac{\partial THG}{\partial z}}{\sqrt{\left(\frac{\partial THG}{\partial x}\right)^2+\left(\frac{\partial THG}{\partial y}\right)^2}}\right)-1\right)+1\right]} \quad (6)$$

In equation (6), $\frac{\partial THG}{\partial z}$ is the vertical derivative of THG, $\sqrt{\left(\frac{\partial THG}{\partial x}\right)^2+\left(\frac{\partial THG}{\partial y}\right)^2}$ signifies the amplitude of the horizontal derivative of THG, and the α value is a positive number chosen by the interpreter, ranging from 2 to 10 [2, 14]. The improved LTHG or IL method provides a maximum amount over the edges of the buried bodies [14].

Melouah and Pham (2021) introduced the improved LTHG filter (ILTHG) by employing the upward continuation (UC) filter along with the vertical gradient of gravity and magnetic data. The purpose of this filter is to mitigate noise and enhance the identification of deep sources. The improved version of the total horizontal derivative logistic function (ILTHG) is outlined as follows [15]:

$$ILTHG=\left[1+\exp\left(-\frac{\frac{\partial ITHG}{\partial Z}}{\sqrt{\left(\frac{\partial ITHG}{\partial x}\right)^2+\left(\frac{\partial ITHG}{\partial y}\right)^2}}\right)\right]^{-\propto} \quad (7)$$

where the ITHG of the gravity and magnetic data is expressed by:

$$ITHG=\sqrt{\left(\frac{\partial VD}{\partial x}\right)^2+\left(\frac{\partial VD}{\partial y}\right)^2} \quad (8)$$

In equation (8), VD is the vertical gradient of anomaly. Similar to the other filters based on the logistic function (LTHG and IL), the ILTHG approach yields maximum amplitudes over the edges of the buried source [2, 4, 15].

To assess the effectiveness and capacity of the aforementioned filters, with a specific focus on the three filters used to identify the boundaries of concealed sources through the logistic function (LTHG, IL, and ILTHG), a preliminary step involved creating two synthetic models of gravity and magnetic data shaped as prismatic structures, incorporating both positive and negative anomalies. These models were intentionally injected with Gaussian noise to examine the robustness of the filters and their performance in detecting edges. After testing and comparing the gravity and magnetic anomaly edge detection filters, we applied the measured complete Bouguer anomaly (CBA) data to Slovakia. In addition to the gravity map, the geological map is also used as a case study to verify the results obtained. The primary aim of this research is to contrast the effectiveness of logistic-based edge detection filters with traditional ones and assess the filter quality when subjected to noisy conditions. A comparative analysis of these filters, both in the presence of noise and using both synthetic and real-world field data, serves as a suitable criterion for identifying the most suitable filter for delineating the horizontal boundaries of subsurface geological formations.

3. Synthetic Models Contaminated with Noise

In order to evaluate the efficacy of the the filters mentioned, a MATLAB environment was used to generate two synthetic gravity and magnetic models. These models were intentionally subjected to Gaussian noise. The initial phase involved evaluating the filters' performance in identifying the boundaries of concealed sources within an artificially generated gravity model. This model encompassed varying parameters, delineating positive and negative density contrasts. Subsequently, the filters' capability to detect the boundaries of

submerged sources within a synthetic magnetic model was examined. This model featured diverse geometric parameters and magnetization properties.

3.1. Gravity Data

In the initial scenario, a synthetic gravity model was constructed, incorporating randomly applied Gaussian noise with a mean of zero and a standard deviation equivalent to 3% of the data's amplitude. Figure (1) presents both top and three-dimensional perspectives of the synthetic gravity model. The specifics of the model's parameters can be found in Table (1). This synthetic gravity model was generated on a structured grid measuring 301×301 in the north-south (N-S) and east-west (E-W) directions, with a sampling interval of 1 km. The gravity anomaly map, along with outcomes derived from employing various filters for edge detection – encompassing THG, AS, TA, TM, LTHG, IL, and ILTHG filters – are depicted in Figure (2).

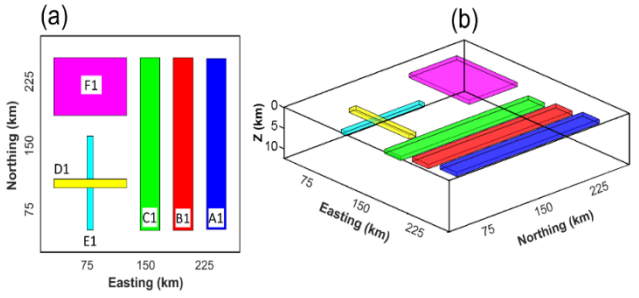

Figure 1: a) two-dimensional view of the first synthetic model along with the labels of different sources, b) three-dimensional view of the first synthetic model.

Table 1: first model with different geometric parameters and densities.

Parameters/Model label	A1	B1	C1	D1	E1	F1
X-coordinates (km)	150	150	150	95	95	230
Y-coordinates (km)	265	210	165	75	75	75
Length (km)	240	240	240	110	130	110
Width (km)	30	30	30	11	10	78
Density (g/cm^3)	0.5	-0.5	-0.3	0.3	-0.3	0.4
Top depth (km)	3	4	5	6	5	3
Bottom depth (km)	5	5	6	7	6	4
Strike Azimuth (degrees)	0	0	0	0	0	0

In Figure 2a, the synthetic gravity anomaly is depicted, showcasing the presence of six buried prismatic sources. Figures 2b and 2c offer representations of the lateral boundaries of the gravity model from Figure 2a, discerned using the THG and AS algorithms, respectively. Notably, the delineation of the deep sources (C1, D1, and E1) appears somewhat obscured. Figures 2d and 2e illustrate the outcomes obtained when applying the TA and TM techniques to the synthetic anomaly of Figure 2a. While the zero and minimum contours of TA and TM can trace the edges to some extent, the outcomes are characterized by a certain degree of blurriness. Despite the presence of noise in the dataset, the tilt angle filter still manages to determine the structural boundaries to a reasonable extent.

Moving on, Figures 2f, 2g, and 2h present the outcomes resulting from the application of the LTHG, IL, and ILTHG methods to the data in Figure 2a. However, it's noticeable that the boundaries of the deep sources remain indistinct. Filters grounded in the logistic function (LTHG, IL, and ILTHG) demonstrate sensitivity to noise, making it highly advisable to implement noise reduction filters. Consequently, to mitigate the influence of noise, a 1 km upward continuation (UC) filter was applied to the noisy dataset prior to employing edge detection techniques. Figure 3 illustrates the outcomes of edge detection subsequent to utilizing the upward continuation filter.

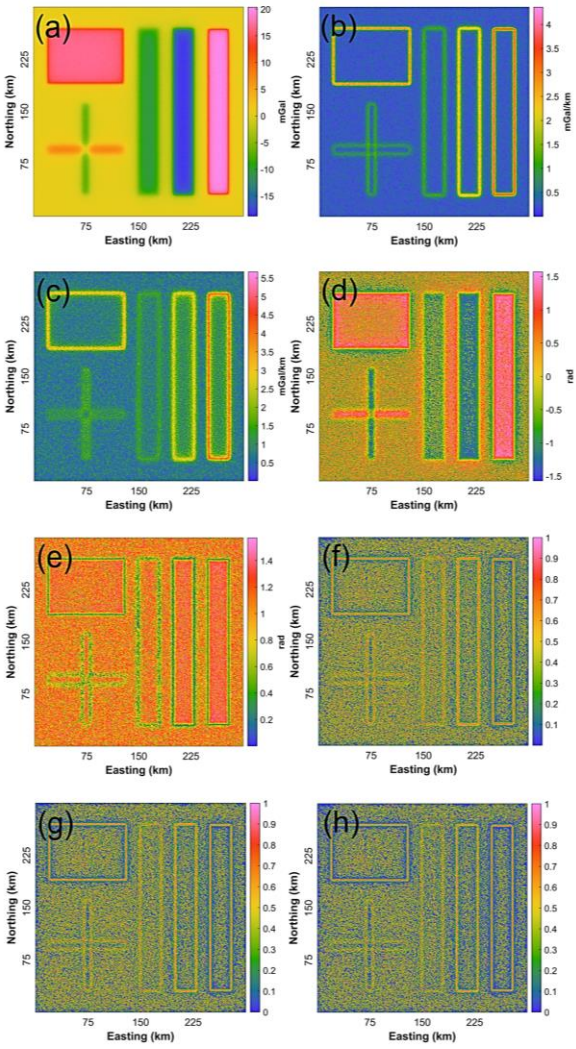

Figure 2: a) synthetic gravity field generated by 6 prismatic sources and subjected to noise, b) THG, c) AS, d) TA, e) TM, f) LTHG (α=2), g) IL (α=2), h) ILTHG (α=2).

In Figure 3a, the gravity anomaly is depicted after being subjected to denoising via an upward continuation filter. Figures 3b and 3c showcase the boundaries of the synthetic gravity dataset from Figure 3a, delineated by means of the THG and AS filters. Notably, the lateral edges of the deeply buried sources (C1, D1, and E1) remain somewhat obscured. Figure 3d portrays the outcomes derived from implementing the TA approach for edge detection on the causative sources from Figure 3a. While the 0° contours of the TA can outline the edges, the boundaries of the slender sources (E1 and D1) are less distinct and slightly exaggerated in size.

Figure 3e demonstrates the outcome of employing the TM filter on the data presented in Figure 3a. The filter successfully identifies all edges, yet a notable drawback is its propensity to introduce false minimal boundaries between sources (such as A1 and B1 or C1 and F1). Turning attention to Figures 3f, 3g, and 3h, the results stemming from the application of the logistic-based filters (LTHG, IL, and ILTHG) to the data in Figure 3a are displayed. Both LTHG and IL filters manage to balance the anomalies arising from deep and shallow sources. From these figures, it is evident that while the LTHG and IL methods offer reasonable estimates for the various amplitude anomaly edges, the logistic function-based filters of total horizontal gradient and improved logistic function exhibit more distinct and precise representation of the balanced anomalies compared to other methods.

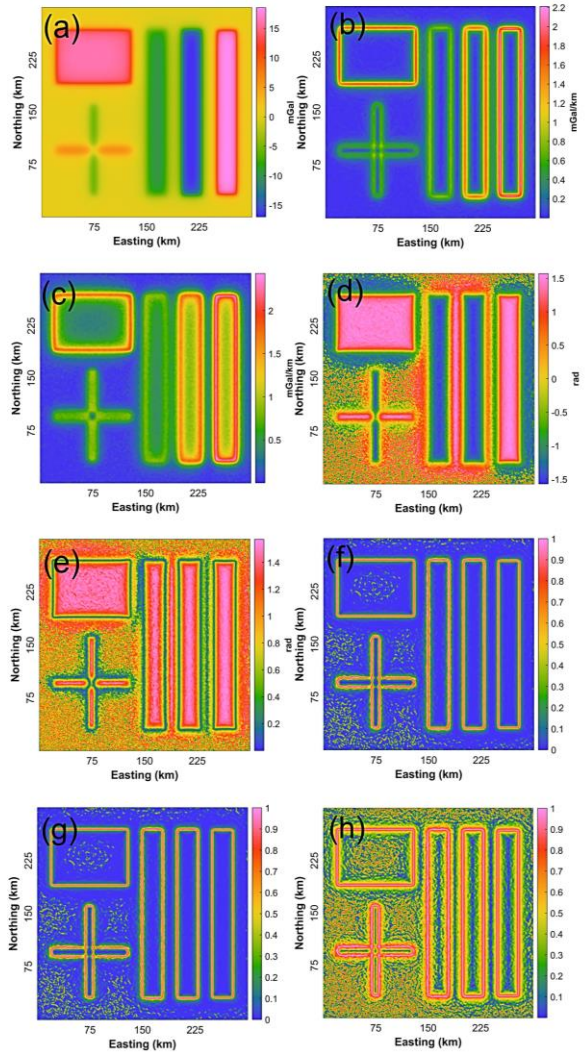

Figure 3: a) synthetic gravity anomaly generated by 6 buried sources after upward continuation of 1km, b) THG, c) AS, d) TA, e) TM, f) LTHG (α=2), g) IL (α =2, h) ILTHG (α=2).

3.2. Magnetic Data

In the subsequent scenario, lateral boundary detection filters were applied to a second model containing random Gaussian noise. The noise exhibited a mean of zero and a standard deviation corresponding to 4% of the data's amplitude. Figure (4) provides both a top view and a 3D view of this second model. Detailed parameters concerning this model are detailed in Table (2). The magnetic anomaly of this second model, characterized by distinct magnetization properties, was computed on a standardized grid of 301×301 units in the north-south (N-S) and east-west (E-W) directions. The sampling interval was established at 1 km. Within this context, the magnetic field's inclination was set at 90°, whereas the declination was assumed to be 0°. The magnetic anomaly map, in conjunction with the results emanating from the application of diverse filters for edge detection, encompassing THG, AS, TA, TM, LTHG, IL, and ILTHG filters, are meticulously presented in Figure (5).

Figure 5a presents the synthetic magnetic anomaly resulting from the presence of six prismatic sources. Figures 5b and 5c illustrate the boundaries of the second model's data in Figure 5a, delineated using the THG and AS algorithms, respectively. However, the D2 source remains undetectable in the THG and AS maps. These filters are notably influenced by the robust amplitude responses of the shallow sources, while the faint amplitude responses from sources A2, B2, C2, and E2 appear blurred.

Table 2: second model with different geometric parameters and magnetization.

Parameters/Model label	A2	B2	C2	D2	E2	F2
X-coordinates (km)	150	50	250	150	150	150
Y-coordinates (km)	270	140	140	15	140	135
Length (km)	150	200	200	160	160	90
Width (km)	21	38	38	7	103	60
Remanent Inclination	90°	90°	90°	90°	90°	90°
Remanent Declination	0°	0°	0°	0°	0°	0°
Magnetization (A/m)	1.1	1	1	1.3	1.2	1.3
Depth of top (km)	4	5	5	6	5	3
Depth of bottom (km)	6	6	7	7	6	4
Strike Azimuth (degrees)	0	0	0	0	0	0

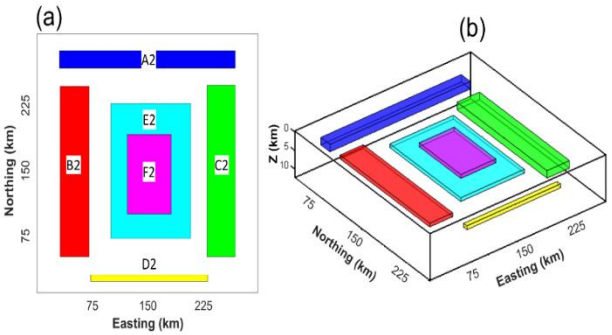

Figure 4: a) two-dimensional view of the second synthetic model along with the labels assigned to different sources, b) three-dimensional view of the second synthetic model.

Moving forward, Figure 5d portrays the outcome of implementing the TA approach to the data in Figure 5a. While the 0° contours of the TA can trace the edges, this outcome falls short in the case of the slender D2 source. In Figure 5e, the results of applying the TM approach are depicted. The TM approach identifies source edges through minimal values rather than zero values. This results in diffuse representation of the weaker amplitude responses from the deeper source (D2). In the presence of data noise, the TA filter exhibits superior resolution compared to the TM filter.

Next, Figures 5f, 5g, and 5h showcase the results generated by utilizing the LTHG, IL, and ILTHG filters on the data in Figure 5a. These filters struggle to accurately delineate the boundaries of significant bodies, leading to the generation of numerous artificial contours in the output maps. A recommendation is to employ an upward continuation filter, particularly when assessing deeper sources, given that the influence of deep magnetic anomalies is considerably less than that of near-surface anomalies.

The purpose of the UC filter is to eliminate short-wavelength anomalies, emphasize deeper anomalies, and diminish the impact of noise. To counteract the influence of Gaussian noise, a UC filter with a radius of 1 km was employed on the noisy data prior to implementing the edge detection process. Figure 6 illustrates the outcomes of the UC filter. In Figures 6b and 6c, the results of edge detection for the second model using the THG and AS methods are displayed, respectively. As observed before, THG and AS continue to struggle with identifying the boundaries of the deep sources.

Turning attention to Figures 5d and 5e, the outcomes derived from applying TA and TM filters are shown. However, these filters generate certain false boundaries that do not align with the lateral edges of the sources. Figures 5f, 5g, and 5h present the edges determined through the LTHG, IL, and ILTHG approaches. The ILTHG filter falls short in defining the boundaries of the slender sources (F2 and D2). Comparatively, the edges delineated by the LTHG and IL filters appear clearer and more precise when compared to outcomes from the THG, AS, TA, and TM methods.

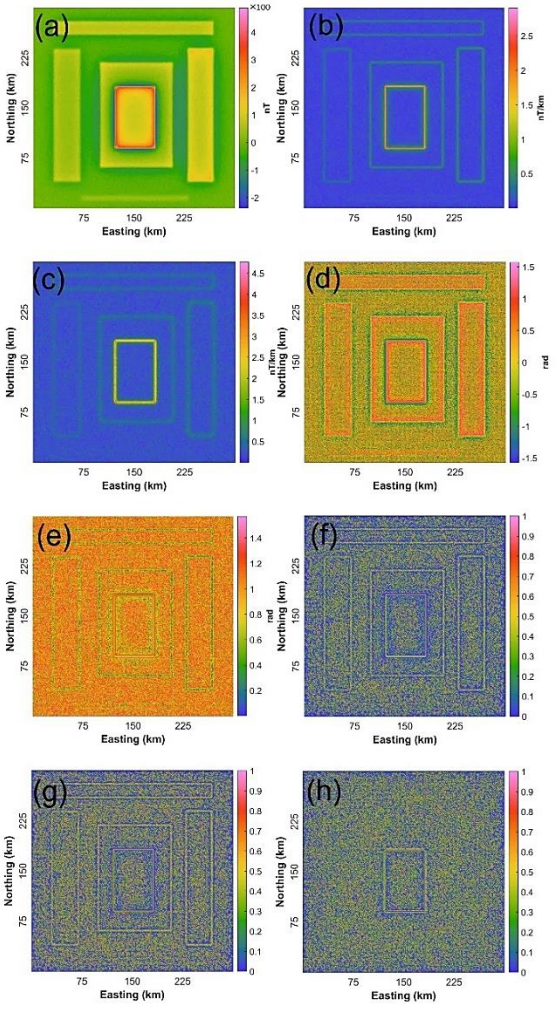

Figure 5: a) second model magnetic anomaly generated by 6 prismatic sources containing Gaussian noise, b) THG, c) AS, d) TA, e) TM, f) LTHG (α=2), g) IL (α =2), h) ILTHG (α=2).

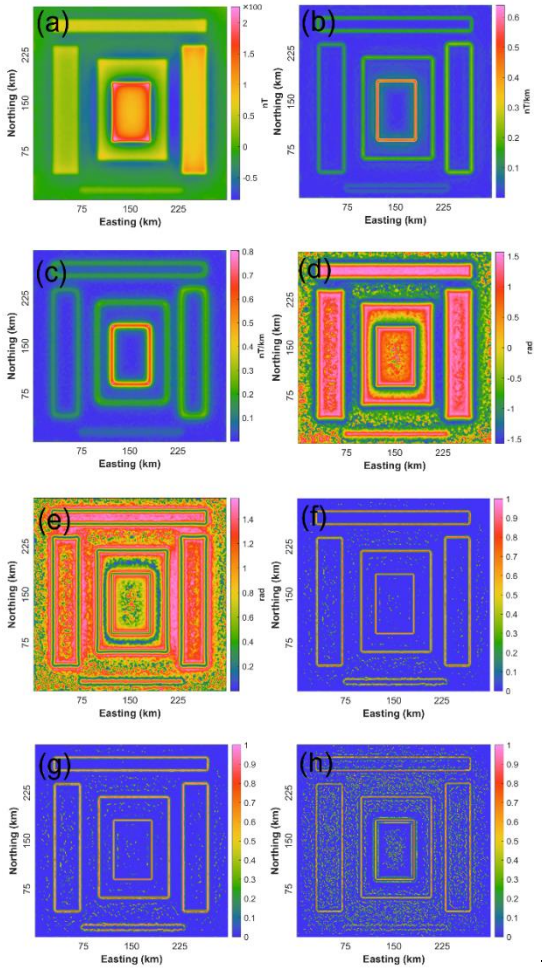

Figure 6: a) second model magnetic field produced by 6 prismatic sources after UC of 1km, b) THG, c) AS, d) TA, e) TM, f) LTHG (α=2), g) IL (α =2), h) ILTHG (α=2).

4. Field Application

This section aims to investigate the suitability of standard and logistic filters in the case ofemploying them on real gravity field data from the Tribeč Mountains and the Pohronský Inovec Mountains in the Western Carpathians (territory of Slovakia).

4.1. Geological Setting

The region of Slovakia is shaped by the Western Carpathians, a mountain range largely attributed to the effects of the Alpine orogeny [25, 26, 27]. Figure 7 presents a simplified geological map portraying the Tribeč mountains and the Pohronský Inovec mountains within the Western Carpathians, highlighting significant fault lines such as Šurany, Mojmírovce, Veľké Zálužie, and Ripňany. The study area's position on the Slovak map is also indicated [29]. The Tribeč mountains exhibit a diverse range of rock types including igneous, sedimentary, and metamorphic rocks (Figure 7). The Paleozoic and Mesozoic sedimentary layers predominantly consist of sandstones, shales, limestone, dolomites, and quartzites [27, 28, 29]. The Rišňovce depression occupies the western portion, while the Komjatice depression is situated to the east of the Tribeč mountains. In contrast, the Pohronský Inovec mountains are primarily composed of andesite lava flows, breccias, and conglomerates [27]. Noteworthy normal faults are observed in the northwest to southeast direction within the Tribeč mountains, particularly in the Danube basin.

4.2. Real Gravity Data

The Bouguer anomaly dataset of Slovakia (SCBA) was compiled from a total of 319,915 observation points [30]. Regional gravity measurements were conducted across Slovakia (with the exception of inaccessible regions) at a scale of 1:25,000, translating to an average of 3-6 points per square kilometer [30]. The region of interest extracted from SCBA lies within UTM coordinates ranging from 530000E to 530000E and 130000N to 1230000N. This area spans approximately 100 km by 70 km. The comprehensive Bouguer gravity data and geological map are accessible online and can be downloaded free of charge from the State Geological Institute Dionyza Stura Bratislava's website. The gravimetric data derived from the Slovak database demonstrate satisfactory quality and can be employed with confidence for interpreting geological formations and geodetic applications [30]. Figure 8a presents the Bouguer gravity anomaly within the area, while Figures 8b and 8c showcase the outcomes yielded by the THG and AS filters, respectively.

As evident, both THG and AS maps are primarily influenced by anomalies present in the Tribeč Mountains and Pohronský Inovec Mountains, potentially arising from shallow structures. Notably, the AS and THG maps exhibit blurriness and unreliability when attempting to discern well-defined boundaries for subsurface sources. Figures 8d and 8e illustrate outcomes stemming from the application of the TA and TM filters, respectively. The TA and TM filters demonstrate a relatively

uniform sensitivity to buried source depth, allowing for effective resolution of both shallow and deep anomalies. This equips these filters to identify anomalies across the study area. Specifically, the TA and TM filters were utilized to ascertain the horizontal positions of shallow and deep sources within the Tribeč Mountains and Pohronský Inovec Mountains, respectively.

Transitioning to Figures 8f and 8g, the results stemming from the utilization of the LTHG and IL techniques are presented. However, outcomes from these filters exhibit a lack of clarity and are characterized by low resolution. The identification of horizontal source locations remains unattainable through these approaches. Figure 8h displays the results obtained through the ILTHG methodology. This approach, rooted in gravity gradient (ITHG) data, the signal amplicates due to noise in the dataset, ultimately leading to suboptimal results. Even modest source boundaries remain ambiguous within this context.

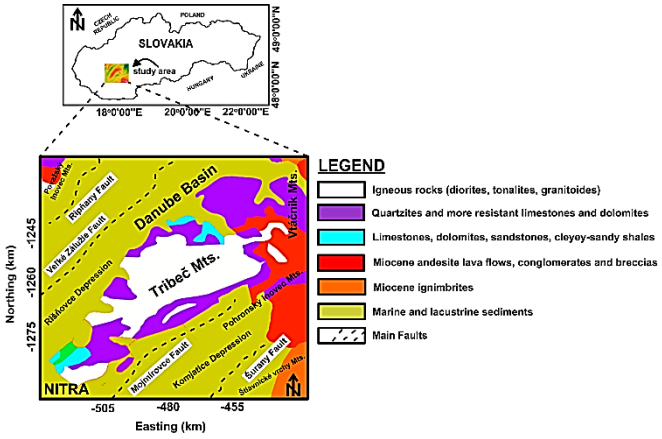

Figure 7: Study area and simplified geological map of the Tribeč and the Pohronský Inovec mountains (based on [28] and [29]). Four main faults (Šurany, Mojmírovce, Veľké Zálužie, and Ripňany) are shown on the map.

In this context, the selection of the 1 km height for the UC filter was made in consideration of achieving a smoothed gravity field map that remains unaffected by local anomalies and noise. Figure 9a portrays the gravity anomalies after undergoing an upward continuation of 1 km. As anticipated, Figures 9b and 9c demonstrate how both THG and AS methodologies prove to be more effective in delineating distinct horizontal boundaries for the subsurface structures within the Western Carpathians.

Subsequently, Figures 9d and 9e present the outcomes yielded through the application of the TA and TM filters, respectively. These filters were specifically utilized to simultaneously visualize both large and small amplitude edges. The results indicate that the TA and TM filters manage to create an evened-out map; however, several adjacent edges become interconnected, leading to the formation of diffuse boundaries. Such outcomes could potentially lead to erroneous structural interpretations and complicate field data interpretation.

Turning attention to Figures 9f and 9g, the results derived from utilizing the LTHG and IL techniques are showcased. Remarkably, the LTHG and IL filters demonstrate significantly higher success compared to the THG, AS, TA, and TM filters in effectively equalizing the amplitudes of anomalies within the Tribeč and Pohronský Inovec Mountains. These approaches exhibit notably stronger gradients over source boundaries. Four primary faults – Šurany, Mojmírovce, Veľké Zálužie, and Ripňany – alongside fault zones and subsurface structures, were identified. Notably, these results are consistent with the geological map depicted in Figure 7.

Concluding this section, Figure 9h showcases the outcomes yielded by the ILTHG approach. Despite employing an upward continuation map, the horizontal boundaries of subsurface resources are ultimately artificial and unreliable.

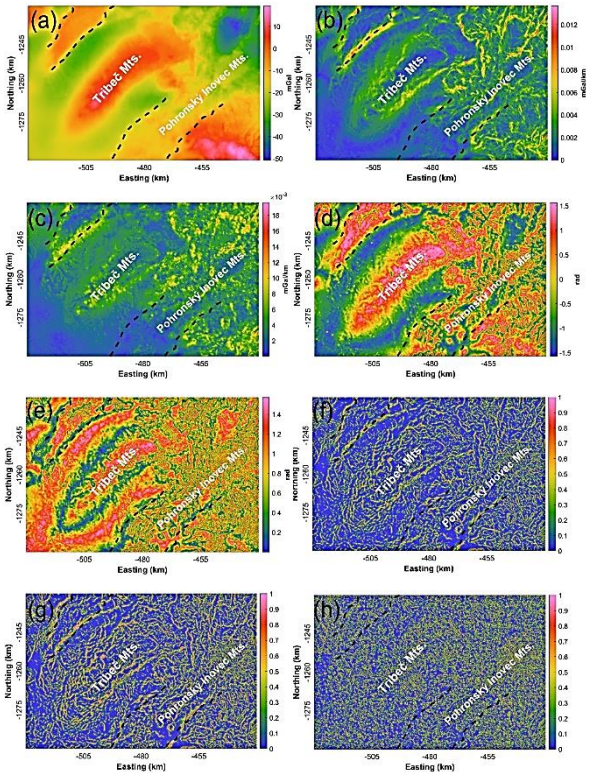

Figure 8: a) gravity anomaly of the Tribeč mountains and the Pohronský Inovec mountains, b) THG, c) AS, d) TA, e) TM, f) LTHG (α=2), g) IL (α =2), h) ILTHG (α=2) (Tribe and Pohronsk Inovec mountains location and four main faults of the study area are shown on the images of edge detection).

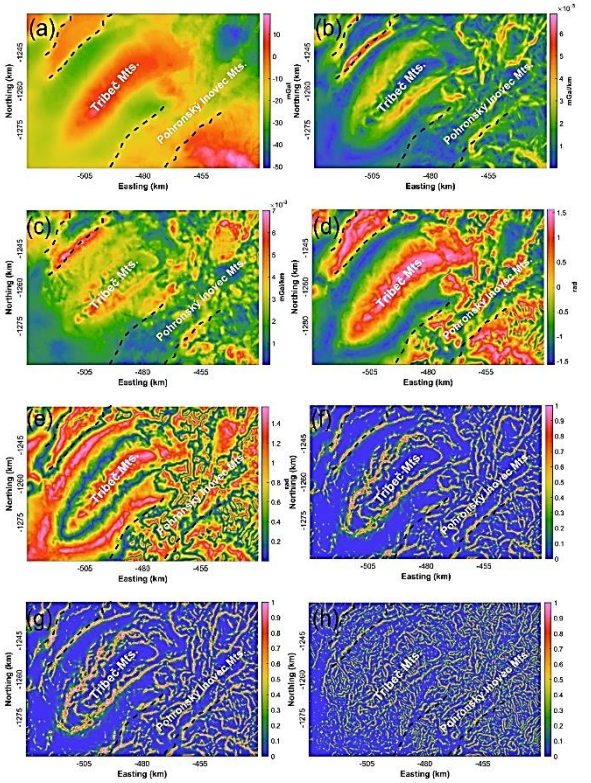

Figure 9: a) SCBA after the UC filter of 1 km, b) THG, c) AS, d) TA, e) TM, f) LTHG with (α=2), g) IL (α =2), h) ILTHG (α=2) (Tribe and Pohronsk Inovec mountains location and four main faults of the study area are shown on the images of edge detection).

5. Conclusions

In the initial phase of the study, synthetic gravity and magnetic models affected by Gaussian noise were employed. Beginning with a gravity model influenced by Gaussian noise, followed by the introduction of noise to a magnetic model, allowed for the evaluation of the edge detection capabilities of standard filters, including THG, AS, TA, TM, and the Logistic algorithm. The outcomes of this investigation revealed that filters based on total horizontal gradient and signal analytics are unsuitable for deep structure determination. Similarly, the filters involving tilt and theta angle exhibited inadequate performance, generating false boundaries. In contrast, the LTHG and IL methodologies demonstrated the ability to precisely outline lateral boundaries. However, the ILTHG filter fell short in meeting the required standard of quality and effectiveness.

Subsequently, the focus shifted towards the application of edge determination filters on real field data obtained from Slovakia. In this context, the LTHG and IL filters showcased superior quality in comparison to alternative filters. The logistic maps produced by the LTHG and IL filters presented clear and informative output images. The significance of utilizing an upward continuation filter cannot be overstated, as its recommendation is strong for achieving desired effects while mitigating the impact of noise. The maps derived from the LTHG and IL methodologies are particularly valuable, effectively highlighting the edges of potential field anomalies when contrasted with the original anomaly map. These maps serve as essential tools for identifying subtle gravity and magnetic anomalies, as well as identifying the locations of subsurface anomalies.

Acknowledgments

The authors thank the state geological institute of Dionyza Stura Bratislava for providing the geophysical data and the report. Dr. Meysam Abedi and Dr. Luan Thanh Pham also for their constructive suggestions to improve the manuscript.

Data Availability Statement

The Bouguer gravity data of Slovakia territory is available at https://www.geology.sk/maps-and-data.

REFERENCES

[1] Hinze WJ, von Frese RRB, Saad AH. Gravity and Magnetic Exploration—Principles, Practices, and Applications. 1st ed. Cambridge University Press; 2013. 525 p

[2] Alvandi, A., Toktay, H, D., & Pham, L, T. (2022a). Capability of improved Logistics filter in determining lateral boundaries and edges of gravity and magnetic anomalies Tuzgolu Area Turkey, Journal of Mining Engineering, 17(56), pp. 57-72. doi: 10.22035/ijme.2022.538985.1889

[3] Everett, M.E. (2013). Near-surface applied geophysics. Cambridge University Press

[4] Alvandi, A., Toktay, H, D., & Pham, L, T. (2022b). Interpretation of gravity data using logistic function and total horizontal gradient (LTHG)-A case study: Charak anticline, JOURNAL OF RESEARCH ON APPLIED GEOPHYSICS (JRAG), 7(5), doi: 10.22055/JRAG.2022.11530.1325

[5] Beiki, M. (2010), Analytic signals of gravity gradient tensor and their application to estimate source location. Geophysics, 75(6): I59-I75.

[6] Bastani M. and L. B. Pedersen, 2001, Automatic interpretation of magnetic dike parameters using the analytical signal technique. Geophysics, 66, 551-561

[7] Haney, M., Johnston, C., Li, Y., and Nabighian, M. 2003. Envelopes of 2D and 3D magnetic data and their relationship to the analytic signal: Preliminary results. In 73rd Annual International Meeting Expanded Abstracts. Society of Exploration Geophysicists, pp. 592–595.

[8] Salem, A., Ravat, D., Gamey, T.J., and Ushijima, K. 2002. Analytic signal approach and its applicability in environmental magnetic investigations. Appl. Geophys., 59, 231–255.

[9] Nabighian, M. N., 1985, Toward a three-dimensional automatic interpretation of potential field data via generalized Hilbert transforms – Fundamental relations. Geophysics, 59, 780-786.

[10] Miller, H.G., and Singh, V.J. 1995. Potential field tilt – A new concept for location of potential field sources. Appl. Geophys., 32, 213–217.

[11] Verduzco, B., Fairhead, J.D., Green, C.M., and MacKenzie, C. 2005. New insights into magnetic derivatives for structural mapping. The Leading Edge, 23, 116–119.

[12] Cooper G R J, Cowan D R. 2006. Enhancing potential field data using filters based on the local phase. Computers & Geosciences, 32 (10): 1585-1591.

[13] Pham, L.T., Oksum, E. & Do, T.D. Edge enhancement of potential field data using the logistic function and the total horizontal gradient. Acta Geod Geophys 55, 153–155 (2019). https://doi.org/10.1007/s50328-019-00258-6

[14] Pham, L.T., Van Vu, T., Le Thi, S. et al. Enhancement of Potential Field Source Boundaries Using an Improved Logistic Filter. Pure Appl. Geophys. 177, 5237–5259 (2020). https://doi.org/10.1007/s00025-020-02552-9

[15] Melouah, O., Pham, L.T., Improved ILTHG method for edge enhancement of geological structures: application to gravity data from the Oued Righ valley, J. Afr. Earth Sci., 177 (2021), Article 105162

[16] Wijns C, Perez C, Kowalczyk P. 2005. Theta map: Edge detection in magnetic data. Geophysics, 70 (5).

[17] Cordell, L., & Grauch, V. J. S., 1985, Mapping basement magnetization zones from aeromagnetic data in the San Juan Basin, New Mexico. In W. J. Hinze (Ed.), The utility of regional gravity and magnetic maps (1st ed., pp. 181–197). Tulsa, Oklahoma:Society of Exploration Geophysicists.

[18] Fairhead, J.D., Salem, A., Williams, S., and Samson, E. 2008. Magnetic interpretation made easy: The tilt-depth-dip- △k method. In 2008 Annual International Meeting Expanded Abstracts. Society of Exploration Geophysicists, pp. 779–783.

[19] Nabighian, M. N., 1972, The analytic signal of two-dimensional magnetic bodies with polygonal cross-section – Its properties and use of automated anomaly interpretation. Geophysics, 37, 507-517.

[20] Nabighian, M. N., 1975, Additional comments on the analytic signal of two dimensional magnetic bodies with polygonal cross-section. Geophysics, 39, 85-92.

[21] Roest, W. R., J. Verhoef, and M. Pilkington, 1992, Magnetic interpretation using the 3-D analytic signal. Geophysics, 57, 116-125.

[22] Salem, A., Williams, S., Fairhead, D., Smith, R., and Ravat, D. 2008. Interpretation of magnetic data using tilt-angle derivatives. Geophysics, 73, L1–L10.

[23] Salem, A., Williams, S., Fairhead, J., Ravat, D., and Smith, R. 2007. Tilt-depth method: A simple depth estimation method using first-order magnetic derivatives. The Leading Edge, 26,

1502–1505.

[24] Hók, J., Kahan, Š. & Aubrecht, R., 2001: Geológia Slovenska. Bratislava, Univerzita Komenského, 1 – 57. (In Slovak.).

[25] Hók, J., Kováč, M., Pelech, O., Pešková, I., Vojtko, R. & Králiková, S., 2016: The Alpine tectonic evolution of the Danube Basin and its northern periphery (southwestern Slovakia). Geol. Carpath., 67, 5, 595 – 505.

[26] Hók, J.; Pelech, O.; Teťák, F.; Németh, Z.; Nagy, A. Outline of the geology of Slovakia (W. Carpathians). Miner. Slov. 2019, 51, 31–60. (THIS IS MISSING IN THE TEXT)

[27] Ivanička J., Polák M., Hók J., Határ J., Greguš J., Vozár J., Nagy A., Fordinál K., Pristaš J., Konečný V., Šimon L., Geological map of the Tribeč Mountains (1:50000). GSSR, Bratislava, 1998.

[28] Bielik, M., Kováč, M., Kučera, I., Michalík, P., Šujan, M. & Hók, J., 2002: Neoalpine linear density boundaries (faults) detected by gravimentry. Geologica Carpathica 53, 235–255

[29] Staškovanová, Veronika and Minár, Jozef. Modelling the geomorphic history of the Tribeč Mountains and the Pohronský Inovec Mountains (Western Carpathians) with the CHILD model, Open Geosciences, 8(1), 2016, pp. 371-389. https://doi.org/10.1515/geo-2016-0038

[30] Zahorec P., Pašteka R., Mikuška J., Szalaiová V., Papčo J., Kušnirák D., Pánisová J., Krajňák M., Vajda P., Bielik M., Marušiak I., 2017: Chapter 7 – National Gravimetric Database of the Slovak Republic. In: Paˇsteka R., Mikuˇska J., Meurers B. (Eds.): Understanding the Bouguer Anomaly: A Gravimetry Puzzle. Elsevier, Amsterdam, 113–125, doi: 10.1016/B978-0-12-812913-5.00006-3.